JOURNAL OF MATERIALS SCIENCE 7 (1972) 303–315

Some Effects of Long Term D.C. Stress on Porcelain Insulators operated at High Temperature

H. GIBSON, J. P. BALLAD
Power Engineering Laboratories, GEC-English Electric, Nelson Research Centre, Beaconhill, Stafford, UK

The deleterious effects resulting from the electrolysis of HV porcelain are discussed with particular regard to the insulation requirements of HVDC mercury valves. Sodium deposition at cathode electrodes and the formation of high resistance "depletion" layers at anode electrodes are examined. Models for the latter are investigated. The desired characteristics of improved insulation materials are outlined and shown to be met by the ceramic now in use.

1. Introduction

In HVDC transmission schemes porcelain insulators are used for a variety of duties such as overhead line insulators and mercury arc valve anode stack insulators. In the latter case the porcelain is required to form a vacuum tight (bakeable) enclosure for the electrode system in addition to providing HV electrical insulation. In some valve designs the porcelain is also required to act as an integral part of the electrode cooling system. These insulators are subjected to DC stresses of about 1 kV/cm and upwards for long periods and (in the case of valve anode stacks) temperatures as high as 150°C.

The electrical properties of HV porcelain insulators operating under such conditions have been observed to deteriorate slowly with time [1-3] as a result of the ionic nature of the conduction current in the porcelain. The ionic leakage currents produce "electrolytic ageing" of the insulator due to: (1) the formation of alkali deposits and conducting dendritic growths at the negative electrodes, and (2) the formation of an ionic depletion layer at the positive electrode leading to a non-uniform voltage distribution over the insulator.

At normal ambient temperatures (~ 20°C) these effects are not usually observed in the lifetime of equipment using porcelain insulators, but since the conduction current through the porcelain increases as an exponential function of temperature, the "ageing" becomes significant at temperatures as low as ~ 80°C, and serious at temperatures as high as 150°C.

Where porcelain is used as vacuum envelopes the electrolytic effects of the conduction current may also lead to vacuum seal failure, this effect has previously been observed in small glass rectifiers by Gallup [4] and others.

After briefly outlining the electrical conduction process in HV porcelain and discussing the phenomenon of thermal breakdown, the bulk of this article is concerned with effects resulting from electrolysis under prolonged DC stress at elevated temperatures. To reduce these effects to an acceptable level, an improved high resistivity ceramic is currently used for HVDC anode stack insulators.

2. DC Conductivity

The electrical conduction process in ceramics of the HV porcelain type is ionic and takes place in the vitreous phase, the dominant charge carriers being Na^+ and K^+. The vitreous phase consists of an irregular network of silicon-oxygen tetrahedra. It is usually assumed that this network is rigid at the temperatures of interest, and that the alkali ions are more loosely bound and reside at various sites in the network. In order to move between vacant sites these ions (cations) have to overcome a potential barrier, and although this will vary between sites an average barrier may be defined for the system. On application of an electric field E, the barrier is lowered in the

direction of the applied field so that thermal vibrations of the ions result in a statistical drift or current flow. For a more detailed discussion see Dekker [5].

For a single species of ion the conductivity may be expressed by

$$\sigma = \frac{A}{T} \exp\left(-\frac{Q}{kT}\right) \quad (1)$$

where Q is the activation energy, k is Boltzmann's constant and T is in degrees Kelvin. Where several species of ion are present the conductivity is given by

$$\sigma = \sigma_1 + \sigma_2 + \sigma_3 + \ldots \quad (2)$$

where $\sigma_1 = \mu_1 n_1 Z_1 e$, etc. and μ_1 is the mobility, n_1 the number density, Z_1 the valency of ion type 1, and e is the electronic charge.

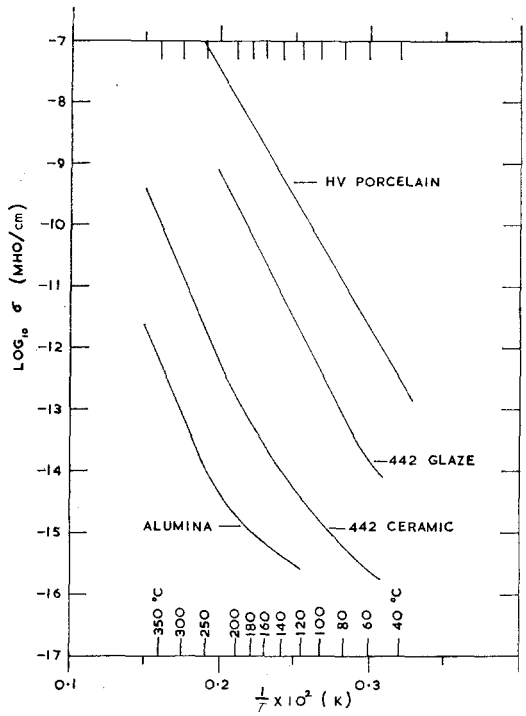

Figure 1 Temperature dependence of electrical conductivity for HV porcelain and Ceramic 442.

A graph of measured values of log σ against $1/T$ for a typical HV porcelain is given in fig. 1. Also shown are graphs for the higher resistivity ceramic currently used in valve anode stacks (442 ceramic), the glaze on that ceramic, and, for comparison, alumina. The conductivity was determined by measuring the current flow through a sample for a range of applied voltages. Sample thicknesses were in the range 2 to 10 mm, and applied voltage stresses in the range 5 to 500 V/mm. Samples had fired-on metal electrodes of either Ag or Pt paste, and types both with and without guard-rings were used. A time delay, varying from one minute for the lowest resistance samples to 15 min. for the highest resistance samples, was allowed to elapse after application of voltage before measurements were made, to allow initial short term charging currents to decay. These arise from ions which can move short distances in the medium before their motion is permanently blocked.

2.1. High Field Conductivity

An attempt was made to observe high field conductivity as observed in glass by Vermeer [6] at field strengths above 10 kV/mm. Using 442 ceramic samples 2 mm thick at 234°C, no departure from linearity of the *V-I* plot was observed up to the maximum voltage stress used of 10 kV/mm.

3. Thermal Breakdown

At elevated temperatures the bulk porcelain undergoes electrical breakdown known as "Thermal Breakdown". This occurs as a result of the temperature dependence of the conductivity expressed in (1) when the voltage stress is raised above the level at which heat generation due to current flow is balanced by heat conduction to the surroundings. O'Dwyer [7] treats the case of voltage applied across a dielectric slab with ends fixed at a temperature T_0. A closer approximation to the practical case of a valve envelope is shown in fig. 2. In this two-dimensional model the inner and outer walls are taken as fixed at the temperature T_0. A constant electric field E causes current flow in the y-direction. The heat generated is conducted to the side walls.

A typical temperature profile (below breakdown) is sketched in fig. 2. The problem is expressed by the heat flow equation:

$$\frac{\partial}{\partial x}\left(K \frac{\partial T}{\partial x}\right) + \sigma E^2 = 0 \quad (3)$$

where K is the thermal conductivity of the porcelain and σ is given by equation (1). Since the thermal conductivity varies only slowly with temperature, decreasing from 0.86 W m^{-1} K^{-1} at 100°C to 0.66 W m^{-1} K^{-1} at 200°C for a typical electrical porcelain, it may be taken as

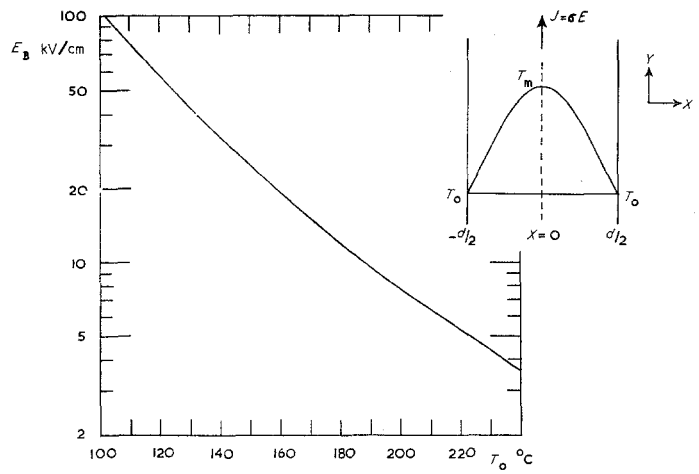

Figure 2 Electric field strength in porcelain for which thermal breakdown occurs, as a function of T_0 with wall thickness $d = 1.0$ cm. Inset: model for analysis of thermal breakdown.

constant compared with the variation of σ with temperature. The resulting differential equation was solved on a digital computer using a finite difference technique and graphs of T_m against T_0 prepared for various field strengths. From these the breakdown field stress E_B was found as a function of ambient temperature T_0. This is plotted in fig. 2 for an HV porcelain wall 10 mm thick.

From the form of the finite difference equation it is found that the breakdown fields can easily be converted for any thickness of wall since $E_B \propto 1/d$ for a given T_0. An alternative model where no heat loss occurs from the inner surface of the valve envelope and the outside surface is kept at temperature T_0 readily follows and yields breakdown field strengths one half of those predicted by the above model.

It is seen from fig. 2 that at 150°C thermal breakdown will not occur at field strengths below 2 kV/mm (c.f. valve operating value of 0.1 kV/mm).

4. Electrolysis of HV Porcelain: Cathode Effects

As a result of DC current flow in the bulk porcelain, alkali ions arrive at the cathode electrode where they are neutralised and accumulate as a metallic deposit. The amount deposited may be calculated from Faraday's laws of electrolysis:

$$m = \frac{W}{ZF} \int_0^t I \, dt \qquad (4)$$

where m is the mass in grams transferred by a varying current I for time t, Z is the valency, W the molecular weight of the charge carriers and $F = 96494$ coulombs.

Stevels [8] shows that the relative activation energies for Na^+ and K^+ depend on the stiffness of the glassy network. From fig. 1 an activation energy of 0.88 eV is obtained for HV porcelain. Comparing this with Stevels data, it is seen that Na^+ will be the dominant carrier. The mass of sodium plated out at the cathode therefore is 2.38×10^{-4} g coulomb^{-1}.

In typical HVDC mercury valves, there are two types of electrode-porcelain contact:
(a) contact via a metal-glass-ceramic seal, as in grid lead-through connectors.
(b) direct contact between the porcelain and platinised grooves in which the grids are supported.

For the first type, sodium plate-out occurs mainly in the glass sealing layer, but at a rate determined by the current flowing through the adjoining porcelain. Prolonged electrolysis has been found to lead to vacuum seal failure. This is due to local strain since when a Na^+ ion is neutralised its diameter increases from 0.95 to 1.86Å [9]. Fig. 3 shows a section through a seal which failed after passing an average charge of 2.2 C cm^{-2} over a period of 47 h at 200°C. The same charge density would result after 600 h at 150°C and 0.1 kV/mm. Aqueous leaching of the fractured seal recovered 5.5 mg Na and 1.6 mg K, indicating that a considerable amount of the deposit must have extended as dendrites into the

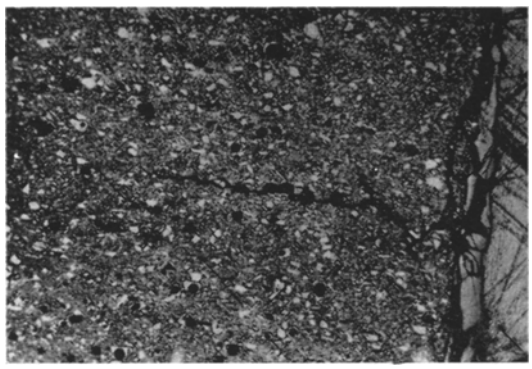

Figure 3 Photomicrograph of a section of HV porcelain/glass/metal seal after long term DC stress at 200°C. (40 ×).

porcelain as shown in fig. 3.

For contacts of the second type, sodium deposition can cause destruction of the platinum coating resulting in the introduction of sodium impurities into the mercury valve. Fig. 4 shows the platinum cathode of a porcelain sample after long term DC stress in air at 0.1 kV/mm, 150°C. The numerous white blobs are sodium salts due to sodium penetration of the platinum layer.

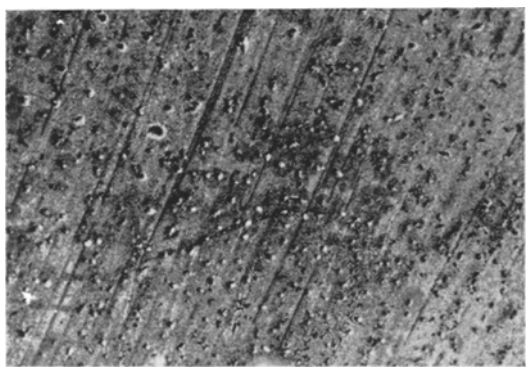

Figure 4 Photograph of platinised end electrode of 10 mm long 20 mm diameter HV porcelain test sample after electrolysis. (9 ×)

Under prolonged electrolysis, dendritic sodium trails growing out from the cathode have been observed to extend so far across the sample that breakdown occurs from the resulting local high stress. The effect is shown in fig. 5 for a sample stressed in air at 0.1 kV/mm, 200°C for 850 h. With another sample stressed under vacuum at 0.2 kV/mm, 150°C for 1000 h breakdown also occurred. In addition a dendrite had penetrated the sample wall and a metallic globule had formed. This was found to be 99.7% sodium with 0.3% potassium.

Dendrite growth has been found to be non-linear with time. For instance, for the sample shown in fig. 5 they had reached the first band at 5 mm distance in about 600 h (as evidenced by short-circuit to the cathode), and had grown right across the 50 mm length in a further 300 h. It is thought that dendrite propagation is assisted by thermal instability produced by local concentrations of current at the dendrite tip, and that consequently the phenomenon may well be exaggerated in accelerated ageing tests conducted at temperatures and field stresses above those expected in practice.

5. Electrolysis of HV Porcelain: Anode Effects

Perhaps more important are the effects of electrolytic ageing which occur at the porcelain-anode junction. These result from the fact that electrodes made from metals which can be used in a mercury environment have ions which are relatively immobile in the porcelain medium. Thus, as current flows through the sample, sodium ions migrate towards the cathode, leaving behind, adjacent to the anode, a layer depleted in sodium ions, hereafter referred to as the "depletion layer". The evidence for the presence of this layer and its main characteristic features are given below. Most of the work reported was performed in air at temperatures up to 200°C, using porcelain disc samples with thicknesses in the range 2 to 50 mm. Unless otherwise stated, the electrodes were of fired on platinum paste (Engelhard 6082), to which contact was made by nickel foil held in compression.

5.1. Current Decay and Voltage Distribution

As electrolysis proceeds the current flowing through the sample decreases. This is shown in fig. 6 for a typical sample stressed with 350 V across its 10 mm length at 200 ± 2°C. At the same time an increasing fraction of the applied voltage becomes concentrated across a thin layer next to the anode electrode. This is illustrated by voltage distribution plots along the surface of a porcelain sample, taken at intervals during electrolysis (fig. 7). These plots were performed with a needle probe connected to a low leakage potentiometer. The sample was fixed on a moving carriage in a controlled temperature enclosure, the probe being lowered onto the sample for the duration of each measurement only. It was

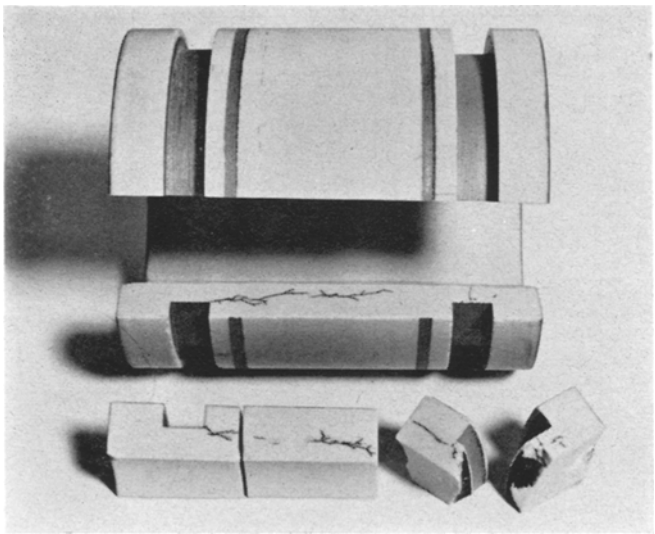

Figure 5 Photograph of 2″ ID 3½″ long test sample of HV porcelain after 850 h at 200°C with 5 kV DC applied to recessed electrodes. Upper electrode positive. Sample sectioned to show internal breakdown path.

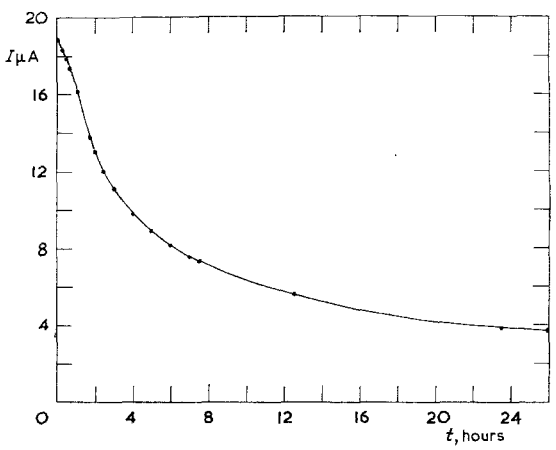

Figure 6 Decay of current with time for HV porcelain disc sample 20 mm diameter 10 mm long with platinised ends. Stressed at 350 V, 200° C ± 2° C.

found that the depletion layer thickness was less than the limit of measurement of the system, namely 0.2 ± 0.2 mm.

5.2. Voltage Reversal

Also shown in fig. 7 are the voltage distributions after reversing the applied voltage. It is observed that the voltage drop at the one end of the sample diminished whilst a depletion layer grew at the other. The way in which the voltage drop at each sample end changed with successive reversals of voltage is shown in fig. 8, together with the current

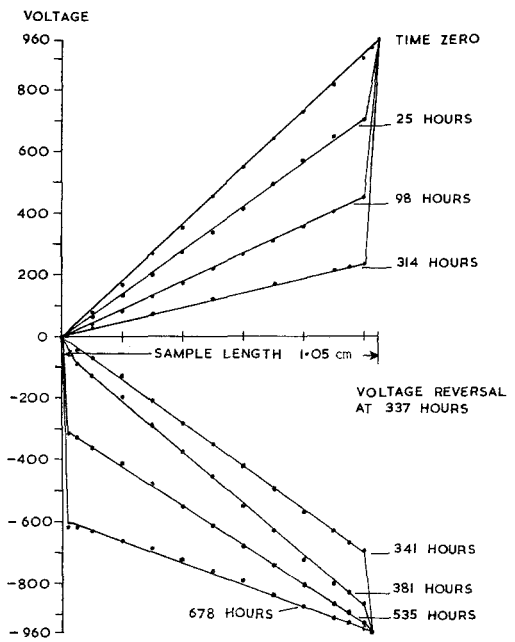

Figure 7 Voltage distribution as measured using potentiometer and probe along a 20 mm diameter, 10.5 mm long HV porcelain sample.
Temperature: 155 ± 5° C. Applied voltage
+ 960 V, $t = 0$ to 337 h
− 960 V, $t = 337$ to 678 h

flowing. The main features demonstrated are: firstly, that provided the temperature was kept

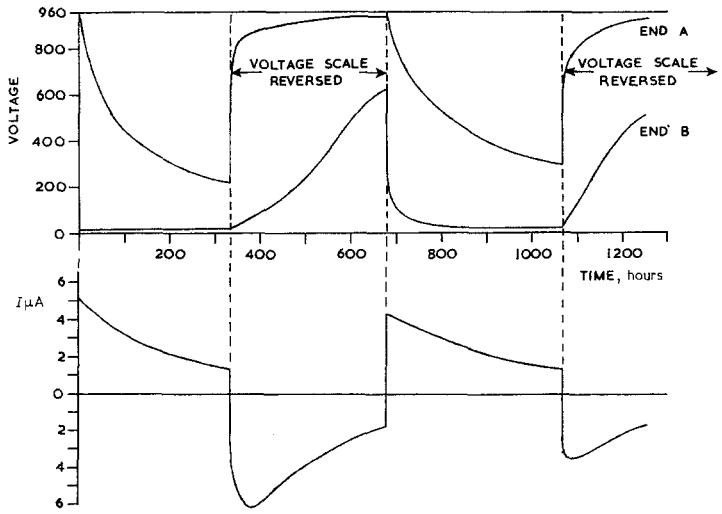

Figure 8 Time variation of voltage 0.5 mm from each end of 10.5 mm long sample, with 960 V applied across it, during successive reversals of voltage. Corresponding variation of current through the sample also shown. Temperature 155 ± 5° C.

constant, the current flowing was proportional to the applied voltage less that dropped at the ends; secondly, that after voltage reversal, the voltage drop in the depletion layer decayed much more quickly than it built up in the forward direction For instance, it took the passage of 3.0 C to build up a depletion layer drop of 730 V, but only 0.3 C in the reverse direction to reduce this to 130 V. Recent results have shown that immediately after voltage reversal (after an initial transient of about 30 sec) the shape of the voltage distribution is almost a mirror image of that just prior to reversal, but the depletion layer voltage drop may be nearly halved by reversal.

5.3. I-V Plots and Effect of Ambient Pressure on Same

As the electrolysis of a sample proceeds its I-V plot becomes increasingly non-linear. This is illustrated in fig. 9 for (a) a sample polarised in air at 150° C and (b) one of a pair of samples polarised under vacuum at 200° C. These "quasi-static" I-V plots were taken by either increasing the applied voltage slowly whilst displaying current and voltage on an oscilloscope screen, or by increasing the voltage in steps and allowing about one minute to elapse before reading the current on an electrometer. In this way dynamic changes (e.g. charging or discharging of capacitative elements) were excluded. The dynamic I-V characteristics are more complex and show large hysteresis effects.

Because it was thought that external leakage through the ambient gas might be important, I-V plots as a function of pressure at a fixed temperature were prepared for one sample. This particular sample had platinum electrodes to which contact was made by nickel wires attached with silver cement. The results are shown in fig. 10. It was found that there was a basic curve which was virtually the same at atmospheric pressure as under high vacuum. At intermediate pressures the *I-V* curves branched away from this basic curve, the breakaway point occurring at lower voltages as the pressure was reduced. At the breakaway point (and above) radiofrequency noise at 1 M Hz was detected on a probe placed near the anode, and on the current signal. This was attributed to corona loss in air. By preparing a graph of the breakaway voltage against pressure and comparing with the right hand branch of the Paschen curve for air, it was estimated that the length over which the leakage occurred was about 1 mm. A similar conclusion was obtained with electrolysed metal-glass-porcelain seal assemblies by considering the onset of noise on the current signal as a function of pressure. One striking example of external leakage across the depletion layer in air was in an experiment on a seal assembly where a rectified AC waveform was used. As a result of repetitive discharges

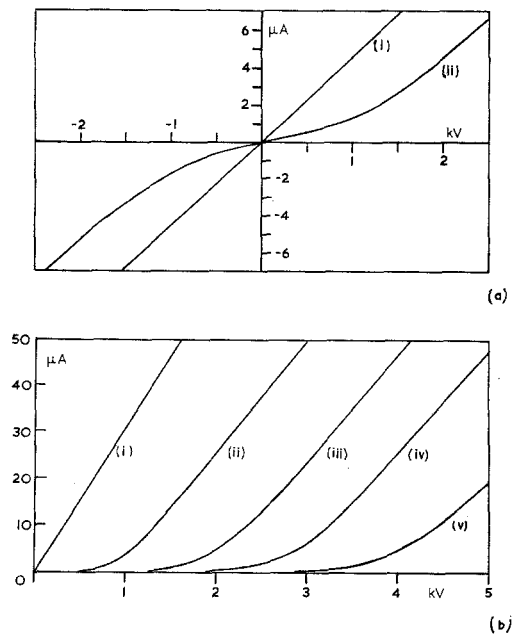

Figure 9 (a) *I-V* plots for 10.5 mm long HV porcelain sample at 155°C. (*i*) without polarisation, (*ii*) after polarising for 337 h at 1 kV (charge passed 2.9 C).
(b) *I-V* plots for 10 mm long sample during polarisation under vacuum at 200°C. (*i*) without polarisation, (*ii*) after 10 h at 1 kV, (*iii*) further 20 h at 2 kV, (*iv*) further 25 h at 3 kV (*v*) further 70 h at 4 kV (total charge passed 0.69, 1.9, 3.2, 6.6 C).

between the positive electrode and the glazed insulator surface, local destruction of the glaze occurred.

Since corona loss cannot occur under high vacuum, it must be concluded that, whilst external leakage through the ambient gas at moderate pressures can occur, the basic shape of the *I-V* curve is fundamental to the depletion layer.

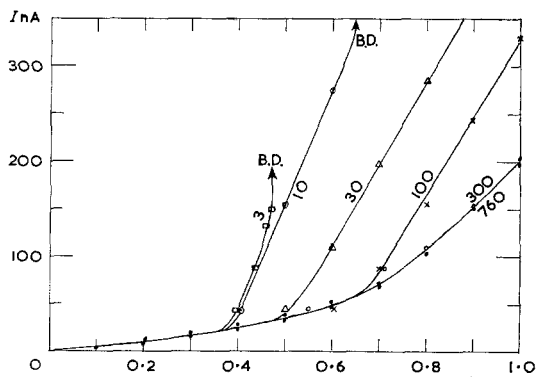

Figure 10 I-V plots for 10 mm long HV porcelain sample after electrolysis, as a function of pressure. Temperature 125°C. Curves labelled in Torr. Breakdowns indicated are those for Paschen breakdown between electrodes.

5.4. Dynamic Response of Depletion Layer

In order to investigate the dynamic response of the depletion layer, the following experiment was performed with a 20 mm diameter, 50 mm long porcelain sample. This had previously been stressed at 350 V and 200°C for 120 h during which 0.77 C were passed.

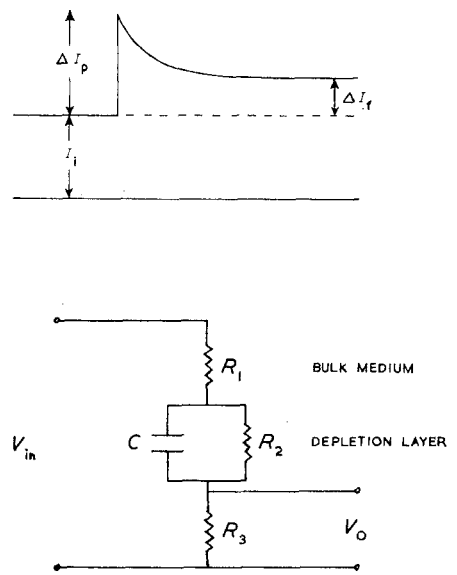

Figure 11 (a) Typical current trace on increasing sample applied voltage by a 30 V step.
(b) Equivalent circuit to explain dynamic response of depletion layer to small voltage steps.

With a given initial DC level, the applied voltage was increased by a 30 V step, and the current flowing was monitored by displaying on an oscilloscope the voltage developed across a 500 k ohm resistor in series with the sample. The current trace (fig. 11a) is recognised as a DC step plus an exponentially decaying transient. The experiment was performed for a range of initial values of applied voltage. It was found that ΔI_p was independent of position on the *I-V* curve. Both I_i and ΔI_f increased as one proceeded up the *I-V* curve, whereas the transient time constant decreased. The system could be described by the equivalent circuit shown in fig. 11b, where *C* in parallel with the variable resistor R_2 represent the depletion layer. This gives:

$$\frac{V_0}{V_{in}} = \frac{R_3}{R_1 + R_3} \exp^{-t/\tau} + \frac{R_3}{R_1 + R_2 + R_3} (1 - \exp^{-t/\tau})$$

where $$\tau = \frac{CR_2(R_1 + R_3)}{R_1 + R_2 + R_3} \quad (5)$$

Results taken at 171°C gave:

$R_1 = 375\ M\Omega$, $R_3 = 500\ k\Omega$, $C = 0.017\ \mu F$, R_2 decreasing as follows:

Initial voltage	50	150	250	350	450	550	650
R_2 MΩ	1125	625	625	292	170	87	54

It is noted that for small steps R_2 is equal to $\Delta V/\Delta I$ at the voltage concerned rather than V/I, where V and I are the steady values for R_2. Similar behaviour was obtained at 200°C and the same value of capacitance of 0.017 μF derived with $R_1 \sim 100\ M\Omega$. With a depletion layer thickness of 3×10^{-2} mm. C^{-1} (see later section), this value of C yields a dielectric constant for the depletion layer of 140. This value is not unreasonable since capacitance bridge measurements on unpolarised porcelain samples have shown the dielectric constant to increase from a frequency independent value of 6 at room temperature to values at 220°C which increased with decreasing frequency, typically 31 at 100 Hz. This behaviour is typical of dipolar relaxation [5, 8].

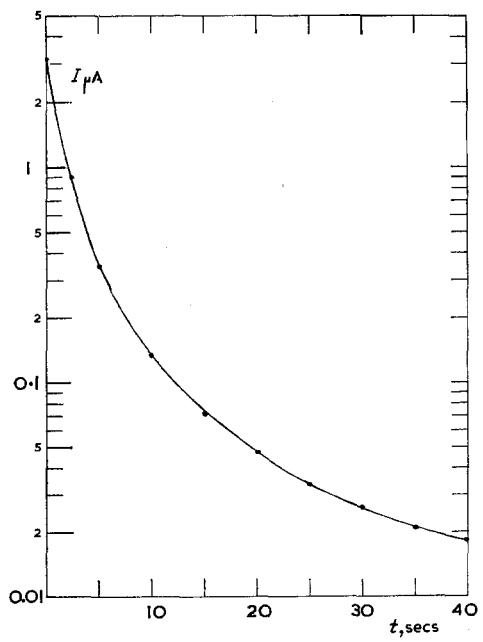

Figure 12 Current flow in reverse direction on shorting the input terminals of a 50 mm long sample after electrolysis. Shorting from 500 V at 200°C.

5.5. Short Circuit Tests

These tests were performed on the same sample as the above dynamic tests, though the behaviour displayed was characteristic of all samples. With the sample passing its quasi-equilibrium current at a given voltage and temperature, the voltage input terminals were short-circuited. The resulting current flow is shown in fig. 12 for shorting from 500 V at 190°C. Consideration of the current flows at 500 V before and after electrolysis, 5.1 μA and 1.9 μA respectively, indicates that about 300 V of the applied voltage would be across the depletion layer. It is then found that the initial part of the short circuit current trace can be explained by discharging C through R_1 in parallel with a changing R_2 (using values interpolated from the above data at 171°C and 200°C). The persistence of current flow beyond about 10 sec must be due to a distribution of dielectric relaxation times, as for instance found by Taylor [10].

5.6. Electron Microprobe Analysis

Analyses conducted on samples sectioned after electrolysis at 160 and 200°C have demonstrated the presence of a layer depleted in sodium next to the anode. The thickness of the layer was proportional to the charge passed. For samples of 20 mm diameter the layer advanced at about 3×10^{-2} mm C^{-1}. It was found that the depletion layer front advanced in a uniform manner with no indication of dendritic growths, the only irregularities being grains imbedded in the vitreous phase (fig. 3). A layer depleted in potassium was also found next to the anode, generally about $\frac{1}{8}$ to $\frac{1}{4}$ of the thickness of the sodium depletion layer.

If it is assumed that the current flow is completely ionic with sodium ions as the dominant carriers, an estimate of the ion density may be made, using the formula

$$Ne\ A\ \delta = q$$

The value obtained is $N \sim 7 \times 10^{20}$ carriers per cms^3, giving a mean interionic distance of about 1.10 nm. By comparison the number density of sodium atoms calculated from the chemical composition and density of the porcelain is

$\sim 8 \times 10^{20}$ per cms^3, indicating that nearly all the sodium ions took part in conduction.

Attempts were made to see if any ions from the electrode material had entered the depletion layer. For samples where nickel wires had been attached to the platinum electrodes with silver cement, it was found that silver ions had entered the porcelain and occupied the depletion layer. For samples without the silver cement (most samples) no evidence of any electrode ions having entered the medium was found.

5.7 Electrolysis Under Vacuum

A pair of 10 mm long, 20 mm diameter samples, connected in parallel, were electrolysed at 200°C in a high vacuum chamber with a mass spectrometer connected. The samples were stressed at 1 kV for a number of hours, then at 2 kV, 3 kV, and 4 kV. The *I-V* plots shown in fig. 9b were taken during this test. It was found that there was copious emission of oxygen whilst current flowed through the sample, and that for a given current flow the oxygen released increased with voltage across the sample.

6. Depletion Layer Models

The data given in section 5 have clearly demonstrated the presence of a depletion layer next to the anode. A satisfactory model would have to explain the observed characteristics of the layer; in particular: the form of the current decay with depletion layer growth, the fundamental *I-V* characteristic at a given thickness of layer, the dynamic response of the layer, and its behaviour under reverse voltage and short circuit conditions. A number of models have been investigated and the simplest way of comparing them is in terms of the predictions of current decay with depletion layer growth. In the descriptions given below it is assumed that δ, the depletion layer thickness, is small compared with d, the sample thickness.

Model 1 Blocking anode, frozen negative ions.

In this model, the mobile positive ions move back as a block from the anode uncovering stationary negative ions. This causes a voltage drop across the depletion layer which can be found by solving Poisson's equation. The growth of the layer is given by

$$\frac{\mathrm{d}\delta}{\mathrm{d}t} = \frac{\mu_+}{\mathrm{d}} \left(V - \frac{g}{2} \delta^2 \right) \qquad (6)$$

where

$$g = \frac{4\pi n_0 e}{\epsilon} ,$$

V is the applied voltage, μ_+ the positive io mobility, n_0 the number density of negative ion: e the electronic charge and ϵ the dielectri constant.

Model 2 Blocking anode, non-stationary nega tive ions.

In this model the positive ions move back as slab, but the negative ions uncovered, whil relatively immobile, are able to move in the hig electric field in the depletion layer. To obtain solution, a partial non-linear differential equ tion for the potential in the depletion layer w generated from Poisson's equation and th current continuity equation. This was solved b the Method of Characteristics [11], yielding fo

$$\mu_- g \delta \gg \frac{\mathrm{d}\delta}{\mathrm{d}t}$$

the following equation for the depletion lay growth:

$$\left(\frac{d}{\mu_+} \frac{\mathrm{d}\delta}{\mathrm{d}t} - V \right)^2 = \frac{8}{9} \frac{g \delta^3}{\mu_-} \frac{\mathrm{d}\delta}{\mathrm{d}t} \qquad (7)$$

Model 3 Electrically neutral, high resistan depletion layer.

Here it is assumed that the negative charges the layer are neutralised in some way (e.g by th inflow of electrode ions), and that the corre conditions occur at the boundary with the bu medium to maintain current continuity. Thus th depletion layer is considered as a thin slab resistivity ρ_1 which is much greater than th resistivity ρ_2 of the bulk medium. The lay growth is given by:

$$n_0 e \frac{\mathrm{d}\delta}{\mathrm{d}t} = \frac{V}{\rho_2 d + (\rho_1 - \rho_2) \delta} \qquad (8)$$

Since $$I = n_0 e \frac{\mathrm{d}\delta}{\mathrm{d}t} ,$$

it is possible to prepare log-log plots of I/I_0 against $\int I \, \mathrm{d}t$ for each of the above models, as shown in fig. 13. The curves are spaced on an arbitrary scale so that their shapes may be compared. In fact they are drawn so as to coincide at a normalised current of 0.9. The experimental results shown by the full circles represent many porcelain samples with platinum electrodes and also some seal assemblies. The open circles represent one sample with platinum electrodes having wires attached with silver

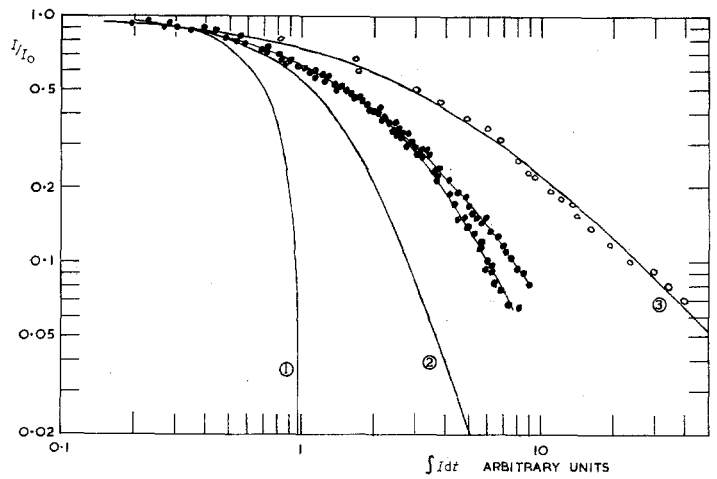

Figure 13 Comparison of experimental results with depletion layer models (model numbers labelled) by plotting normalised current against charge passed. Full circles: Pt electrodes. Open circles: Pt plus Ag cement, or Cu electrodes.

cement, and two samples with copper electrodes formed by electroplating the porcelain. It is seen that, whilst the latter can be fitted by model 3, the bulk of the results lie between models 2 and 3. Furthermore, model 3 will not explain the observed *I-V* characteristics. Thus it is necessary to find a better model.

Model 4 Electrically neutral depletion layer, capable of high-field conductivity.

This model extends the concept of a highly resistive depletion layer in which the current flow is ionic, to include the phenomenon of high-field conductivity, which should occur at sufficiently high field strengths. Following Dekker [5], an expression for the current may be derived:

$$J = \frac{\sigma}{\alpha} \sinh \alpha E \qquad (9)$$

where

$$\alpha = \frac{ae}{2kT}$$

and a is the mean jump distance, or distance between vacant sites. This expression reduces to Ohm's law at low field strengths. The phenomenon would not be observable in porcelain samples several millimeters thick because thermal breakdown would occur at a lower voltage than required to create the sufficiently high field strength. However, with the thin depletion layer this objection does not hold.

The model is sketched in fig. 14. For current continuity we have

$$J = \frac{\sigma_1}{\alpha} \sinh \alpha E_1 = \sigma_2 E_2 \qquad (10)$$

where the subscripts 1 and 2 refer to the depletion layer and the bulk porcelain respectively. Now

$$E_1 = \frac{V - \phi_1}{\delta} \; ; \quad E_2 = \frac{\phi_1}{d} \text{ for } \delta \ll d$$

Substituting in (10) and normalising the equation we obtain

$$\beta \frac{V}{V_0} \frac{\phi_1}{V} = \sinh \frac{V}{V_0} \left(1 - \frac{\phi_1}{V}\right) \qquad (11)$$

where

$$\beta = \frac{\sigma_2 \delta}{\sigma_1 d}$$

and

$$V_0 = \frac{\delta}{\alpha}$$

This equation may be used to predict the quasi-static behaviour of the depletion layer. For a fixed applied voltage V, it is noted that ϕ_1/V represents the normalised current. So by specifying V/V_0 at $\beta = 1$ (say) it is possible to plot a curve of I/I_0 against β. A family of such curves, representing the decay of current with depletion layer growth, is plotted in fig. 14. Equation (11) may also be used to predict *I-V* characteristics. With a fixed δ, which fixes β and V_0, it is noted that

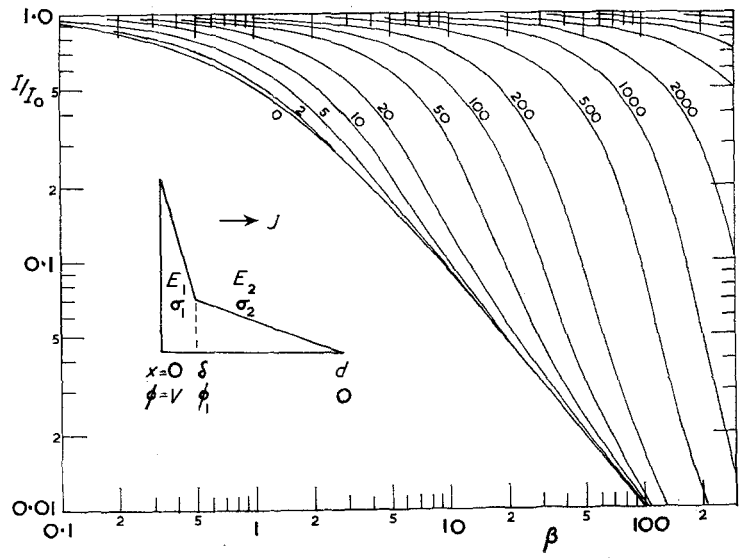

Figure 14 High field conductivity model of depletion layer (inset), showing predicted decay of current with depletion layer growth ($\beta \propto \delta$). Curves labelled with the value of V/V_0 applicable at $\beta = 1$.

$$I \propto \frac{\phi_1}{V} \times \frac{V}{V_0} .$$

Thus *I-V* plots are prepared. A family of curves for different values of β is shown in fig. 15.

It is immediately seen that figs. 14 and 15 show general agreement with experiment. For detailed comparison the *I-V* curves were prepared as log log plots. It was found that there was a certain degree of freedom in matching, and it was necessary to match the current decay and *I-V* data simultaneously to arrive at the depletion layer parameters. The experimental results examined were for the following range of variables; porcelain sample thickness 2 to 50 mm, applied voltage 10 to 1000 V, temperature 150 to 200° C, the current generally falling to 0.2 I_0 after the passage of 0.3 to 3 C.

The values of α found were in the range 10^{-3} to 10^{-2}, yielding jump distances of 3 to 30 nm. These are quite reasonable compared with the mean distance between sodium ions of 1.1 nm. The ratios σ_1/σ_2 covered a wider range from 4×10^{-5} to 3×10^{-3} with a single value outside, namely 2×10^{-6} for the sample electrolysed under vacuum.

Model 4 may be enhanced by consideration of the mechanism causing current continuity at the depletion layer boundary, which would be the formation of a charge layer there. In the forward voltage direction, this would be a negative ion layer between the receding sodium ions and the incoming electrode ions, giving $E_1 = E_2 + 4\pi Q$. Thus E_1 could be much greater than E_2. Provided the charge layer is thin enough for negligible voltage drop to occur across it, it is found that the depletion layer may be represented by a variable resistance R_2 in parallel with a capacitance C, as in fig. 11, where

$$C = \frac{\epsilon A}{4\pi\delta} .$$

Thus the model adequately explains the dynamic behaviour of the depletion layer.

One factor which is not explained is why the current flow on voltage reversal, after an initial transient, should be up to twice that in the forward direction. It should be noted however that the pre-electrolysis state can only be regained after the passage of an equal charge in the reverse direction as passed during electrolysis. This may not be possible if irreversible processes, such as oxygen release, have occurred.

7. Significance for HVDC Valves

In section 4 it was seen that as a result of electrolysis of HV porcelain, a number of effects occur at cathode electrodes which would be undesirable in an HVDC mercury valve. Failure of metal-glass-porcelain seals with consequent loss of vacuum is one such effect. Another is the degradation of fired-on platinum coatings, resulting in the formation of highly resistive contacts and also the release of sodium impurities

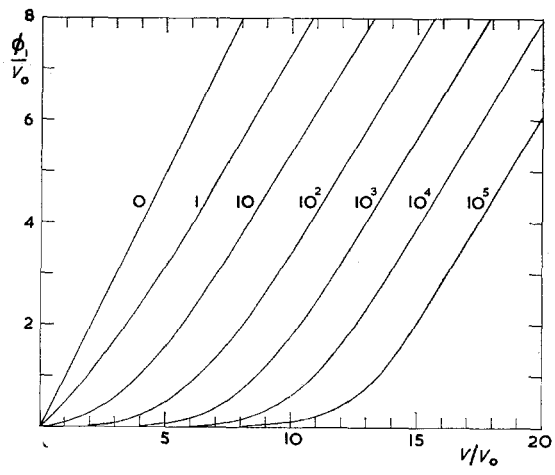

Figure 15 High field conductivity model of depletion layer showing predicted *I-V* curves at various stages of depletion layer growth. Curves labelled with values of β. Note: $I \propto \phi_1$.

into the valve. These effects depend directly on the charge passed and would be reduced to insignificant levels during the life of a valve by the use of a ceramic with resistivity several orders of magnitude greater than HV porcelain.

The principle effect of electrolysis at anode electrodes was seen (section 5) to be that of depletion layer growth, with observed characteristics which could best be explained by a model based on a highly resistive depletion layer in which high field conductivity could take place. One consequence of depletion layer growth which has been discussed is that of external current flow in the ambient air when the voltage across the layer rises to a sufficient value for a type of Paschen breakdown to occur.

One most important result of the presence of a depletion layer is that it can cause serious deterioration of the vacuum breakdown strength across the inner insulator surface. This has been described in detail elsewhere [12] but the main points are summarised below. The vacuum surface DC breakdown level was typically 30 to 40 kV for 10 mm long samples before electrolysis, and these had substantially the same level at 90°C after electrolysis when the voltage was applied in the same direction as during electrolysis. However with the voltage applied in the reverse direction, the breakdown level was considerably reduced and values as low as 5 kV were recorded. Tests on samples electrolysed to values in the range 0.03 to 1 C/cm² showed no dependence on charge passed, and the inference is that the deterioration depends on the presence of a depletion layer rather than its size. Indeed, the theoretical model predicts a depletion layer field E_1, which for $V \gg V_0$ is given by

$$\alpha E_1 = \log_e \left(\frac{2\sigma_2 \alpha}{\sigma_1 d} \phi_1 \right) \simeq \log_e \left(\frac{2\sigma_2 \alpha}{\sigma_1 d} \cdot V \right)$$

which is independent of depletion layer thickness. If this field is high enough to aid electron emission from the new cathode-insulator junction on voltage reversal, significant deterioration of the vacuum surface breakdown level will occur. Lower fields would be expected at the beginning of electrolysis whilst the charge layer at the depletion layer boundary is being established.

Obviously breakdown over valve insulator surfaces must be avoided at all costs since permanent damage to the insulator may result. The external leakage depends on the voltage across the depletion layer (which increases with charge passed) and could be avoided during the life of a valve by the use of much higher resistivity ceramic than HV porcelain. However, the degradation of internal surface breakdown depends on the depletion layer field, which we have seen is not sensitive to charge passed. Whilst it is possible to impede vacuum surface breakdown by shielding the insulator-metal junction and shaping the insulator surface [13], it would be desirable that for any alternative ceramic, even though a depletion layer might grow, the depletion layer field should not be so high as to degrade the surface breakdown strength.

8. Improved Materials for DC Insulation

A material which meets the requirements stated in section 7, whilst still retaining the mechanical characteristics necessary for making ceramic-glass-metal vacuum seals, has been developed at the Nelson Research Centre. This material (Ceramic 442) is currently used in HVDC valve anode stacks. Typical performance is illustrated in the following examples.

In one series of tests, samples consisting of 25 mm cubes with end faces platinised and one side face glazed, so as to simulate a valve envelope, were electrolysed at 1 kV, 270°C for 1000 h during which about 0.2 C were passed through each sample. This is equivalent to welt over 100000 h at normal operating conditions. It was found that depletion layers had grown to a magnitude of ~ 200 V, which is not sufficient to

cause external leakage problems. In addition dendrites had just begun to grow (about 0.5 mm long in the glaze), but this may have been due to accelerated ageing.

In another test an unglazed sample with recessed platinised electrodes 5 cms apart was electrolysed for 7000 h at 150°C with 2.5 kV applied between electrodes. Subsequent vacuum breakdown tests showed no degradation of the surface breakdown level.

Other long term tests on this material (accelerated by the use of higher than normal temperatures) have so far shown no deterioration in its electrical performance or in the vacuum integrity of seals manufactured from it.

References

1. Kh. S. VALEYEV, V. N. GAREVSKII, and N. S. KOSTYOKOV, *Electrichestvo* **1** (1963) 59.
2. Kh. S. VALEYEV, N. G. DROZDOV, and N. K. KNASNOVOLOVII, *Elektricheskie Stantzii.* (1966) 66.
3. G. N. MASLENNIKOVA, N. K. KRASNOGOLOVII, and A. F. BUCHENKOVA, *Glass and Ceramics* **20** (1963) 429.
4. J. GALLUP, *J. Amer. Ceram. Soc.* **20** (1946) 277.
5. A. J. DEKKER, "Solid State Physics" (McMillan Press, London, 1960).
6. J. VERMEER, *Physica.* **22** (1956) 1257.
7. J. J. O'DWYER, "The theory of dielectric breakdown of solids" (Clarendon Press, Oxford, 1964).
8. J. M. STEVELS, "Handbuch der Physik" (Ed. S. Flugge) Vol. XX. (Springer-Verlag. Berlin, 1957) p. 350.
9. E. J. PANNER, *Proc. 5th Nat. Conf. Adv. electron tube tech.* Sept. 1960. pp. 201-203.
10. H. E. TAYLOR, *J. Soc. Glass Tech.* **43** (1959) 124.
11. I. SNEDDON, "Elements of partial differential equations" (McGraw Hill, New York, 1957).
12. H. GIBSON, *Electronics Letters* **7** (1971) 417.
13. M. J. KOFOID, *Trans. AIEE (USA)* Part III **79** (1960) 999.

Received 23 August and accepted 6 October 1971.